OXFORD

Human Molecular Genetics, 2017, Vol. 26, No. 1 173–183

doi: 10.1093/hmg/ddw377
Advance Access Publication Date: 10 November 2016
Original Article

ORIGINAL ARTICLE

Mutation in *VPS33A* affects metabolism of glycosaminoglycans: a new type of mucopolysaccharidosis with severe systemic symptoms

Hidehito Kondo[1], Nadezda Maksimova[2], Takanobu Otomo[1,3,4,*], Hisakazu Kato[5], Atsuko Imai[6,7], Yoshihiro Asano[6], Kaori Kobayashi[7,8], Satoshi Nojima[9], Akihiro Nakaya[7], Yusuke Hamada[1], Kaori Irahara[1], Elizaveta Gurinova[10], Aitalina Sukhomyasova[2,10], Anna Nogovicina[10], Mira Savvina[2], Tamotsu Yoshimori[3,4], Keiichi Ozono[1] and Norio Sakai[1,11,*]

[1]Department of Pediatrics, Osaka University Graduate School of Medicine, Yamadaoka, Suita, Osaka, Japan, [2]Laboratory of Genome Medicine, Clinics of Medical Institute, North East Federal University, Yakutsk, Russia, [3]Department of Genetics, [4]Research Center for Autophagy, [5]Department of Medical Biochemistry, [6]Department of Cardiology, [7]Department of Genome Informatics, Osaka University Graduate School of Medicine, Yamadaoka, Suita, Osaka, Japan, [8]Medical Solutions Division, NEC Corporation, Shiba, Minato-ku, Tokyo, Japan, [9]Department of Pathology, Osaka University Graduate School of Medicine, Yamadaoka, Suita, Osaka, Japan, [10]Republican Hospital no. 1, National Medical Center of the Republic of Sakha, Yakutsk, Russia and [11]Division of Health Science, Child Healthcare and Genetic Science Laboratory, Osaka University Graduate School of Medicine, Yamadaoka, Osaka, Japan

*To whom correspondence should be addressed at: Takanobu Otomo, Pediatrics, Osaka University Graduate School of Medicine, 2-2 Yamadaoka, Suita, Osaka 565-0871, Japan. Tel: +81-6-6879-3932; Fax: +81-6-6879-3939; Email: otomo@ped.med.osaka-u.ac.jp; Norio Sakai, Osaka University Graduate School of Medicine, Division of Health Science, Child Healthcare and Genetic Science Laboratory, 1-7 Yamadaoka, Suita, Osaka 565-0871, Japan. Tel: +81-6-6879-2531; Fax: +81-6-6879-2531; Email: norio@ped.med.osaka-u.ac.jp.

Abstract

Mucopolysaccharidoses (MPS) are a group of genetic deficiencies of lysosomal enzymes that catabolize glycosaminoglycans (GAG). Here we describe a novel MPS-like disease caused by a specific mutation in the *VPS33A* gene. We identified several Yakut patients showing typical manifestations of MPS: coarse facial features, skeletal abnormalities, hepatosplenomegaly, respiratory problems, mental retardation, and excess secretion of urinary GAG. However, these patients could not be diagnosed enzymatically as MPS. They showed extremely high levels of plasma heparan sulphate (HS, one of GAG); 60 times the normal reference range and 6 times that of MPS patients. Additionally, most patients developed heart, kidney, and hematopoietic disorders, which are not typical symptoms for conventional MPS, leading to a fatal outcome between 1 and 2-years old. Using whole exome and Sanger sequencing, we identified homozygous c.1492C > T (p.Arg498Trp) mutations in the *VPS33A* gene of 13 patients. VPS33A is involved in endocytic and autophagic pathways, but the identified mutation did not affect either of these pathways. Lysosomal over-acidification and HS accumulation were detected in patient-derived and VPS33A-depleted

Received: August 26, 2016. **Revised:** October 6, 2016. **Accepted:** October 27, 2016

cells, suggesting a novel role of this gene in lysosomal functions. We hence propose a new type of MPS that is not caused by an enzymatic deficiency.

Introduction

Mucopolysaccharidoses (MPS) are a group of inherited disorders caused by a lack of specific lysosomal enzymes involved in the degradation of glycosaminoglycans (GAG), such as heparan sulphate (HS), dermatan sulphate, keratan sulphate, chondroitin sulphate, or hyaluronic acid (1). Seven types of MPS have been identified, which are caused by deficiencies of 11 different enzymes, as follows: MPS I (Hurler, MIM #607014; Hurler–Scheie, MIM #607015; Scheie MIM #607016), MPS II (MIM #309900), MPS III (IIIA, MIM #252900; IIIB, MIM #252920; IIIC, MIM #252930; IIID, MIM #252940), MPS IV (IVA, MIM #253000; IVB, MIM #253010), MPS VI (MIM #253200), MPS VII (MIM #253220), and MPS IX (MIM #601492). Depending on the enzyme deficiency, the catabolism of different GAG is blocked either singly or in combination. The accumulation of undegraded GAG affects the functions of various cells, tissues, and organs. MPS are heterogeneous and progressive disorders. Patients with MPS typically appear normal at birth, but during early childhood they are clinically characterized by coarse facial features, skeletal abnormalities (dysostosis multiplex), hepatosplenomegaly, respiratory problems, cardiac involvement, mental retardation, and reduced life expectancy. Obstructive airway disease, respiratory infection, and cardiac complications are the usual causes of death commonly in the late teens or early adulthood. Diagnosis of MPS relies on the detection of urinary GAG and deficiencies of specific lysosomal enzymes that degrade GAG, caused by mutations in these enzymes.

In this study, we performed a whole exome and Sanger sequencing in 13 Yakut patients with typical manifestations of MPS, who could not be diagnosed enzymatically as MPS, and found homozygous mutations (NM_022916.4: c.1492C > T, NP_075067.2: p.Arg498Trp) in the vacuolar protein sorting gene *VPS33A* (MIM *610034). VPS33A is a member of the Sec1/Munc18-related (SM) protein family, which is required for SNARE-mediated fusion processes, and is a core subunit of the homotypic fusion and vacuole protein sorting (HOPS) complex. The HOPS complex is involved in both endosome-lysosome fusion and autophagosome-lysosome fusion (2–6). Endocytosis involves the membrane trafficking of exogenous material to intracellular compartments, whereas autophagy involves the membrane trafficking of cytosolic material and their degradation in lysosomes, and both pathways are affected by the knockdown of VPS33A (7). We present a detailed clinical description of the patients and molecular studies suggesting this mutation in *VPS33A* affects not endocytic and autophagic pathways but lysosomal functions involved in GAG metabolism, leading to MPS-like phenotype.

Results

Clinical presentation

Thirteen patients in Yakutia (Sakha Republic in the Russian Federation) were found to have characteristic clinical features of MPS and increased urinary GAG; however, lysosomal enzyme deficiencies were not detected (Fig. 1, Table 1 and Supplementary Material, Table S1). All patients were Yakuts, characterized by specific anthropological, demographic, linguistic, and historical features (8). They were born to non-consanguineous healthy parents, and had obstructive lung disease accompanied by frequent respiratory infection since early infancy. Coarse facial features, macroglossia, thick skin, barrel-shaped chest, psychomotor retardation, hepatosplenomegaly, joint contraction, and progressive skeletal dysplasia (dysostosis multiplex) had developed gradually (Fig. 1A–E). In addition, most patients developed proteinuria, hematopoietic disorders, and congenital heart defects, although these are not typical symptoms of MPS. Eleven of the 13 patients died of cardiorespiratory failure at approximately 1 to 2 years of age. Health information of the deceased patients was based on the retrospective review of medical records. Clinical features of all the patients are summarized in Table 1 and Supplementary Material, Table S1. We investigated the detailed clinical features of one patient (Supplementary Material, Case reports). This patient showed delayed myelination, cerebral calcification, retinal hypopigmentation, and abnormalities in erythroid cell lines, besides dysostosis multiplex (Fig. 1B–I). Autopsy findings of another patient included hypoplastic bone marrow, renal pathological changes, and cerebral calcification, which are also not usually observed in MPS patients (Fig. 1J–L and Supplementary Material, Case reports).

Identification of mutations in *VPS33A*

To identify the causative gene mutation, whole exome sequencing was performed with one family (P12 and his parents; Fig. 2A). The Yakut population exhibits a high frequency of several Mendelian disorders, owing to a founder effect (8–11). Therefore, we assumed the disease-causing mutation to be a homozygous mutation in autosomal recessive inheritance. After applying the filtering criteria described in the methods section, only one protein-altering homozygous variant, c.1492C > T (p.Arg498Trp; hereafter referred to as p.R498W) in the *VPS33A* gene, was identified. Using Sanger sequencing of this mutation in the 13 patients and their unaffected family members, we verified homozygous alterations in all the patients and heterozygous alterations in all their parents, suggesting that this mutation causes a disease with autosomal recessive inheritance (Fig. 2A and Supplementary Material, Fig. S1). The Arg498 residue is highly conserved among species (Fig. 2B). In addition, the p.R498W variant was predicted to be disease-causing by several major algorithms (scaled CADD score v1.3 35, SIFT score 0.001, Polyphen2 score 1, Mutation Taster score 1). The allele frequency of this mutation was reported to be 1 in 59,004 among various ethnic groups in the ExAC database (chr12:122717464 G/A). We analysed 110 healthy Yakuts for this mutation and revealed an allele frequency of 1 in 110. We analysed a region of homozygosity (ROH) using deep sequencing data of patient 12 by the program, HomSI: a homozygous stretch identifier (12). The homozygous variant of *VPS33A* was identified within a 4 Mb ROH in chromosome 12. Altogether, these results imply a regional founder effect, though further experiments are necessary to really assess the possibility of the founder effect.

Massive accumulation of heparan sulphate in patient plasma, fibroblasts, and VPS33A-depleted cells

Patients showed an MPS-like phenotype and increased urinary GAG levels. Therefore, we next investigated the level of HS, one

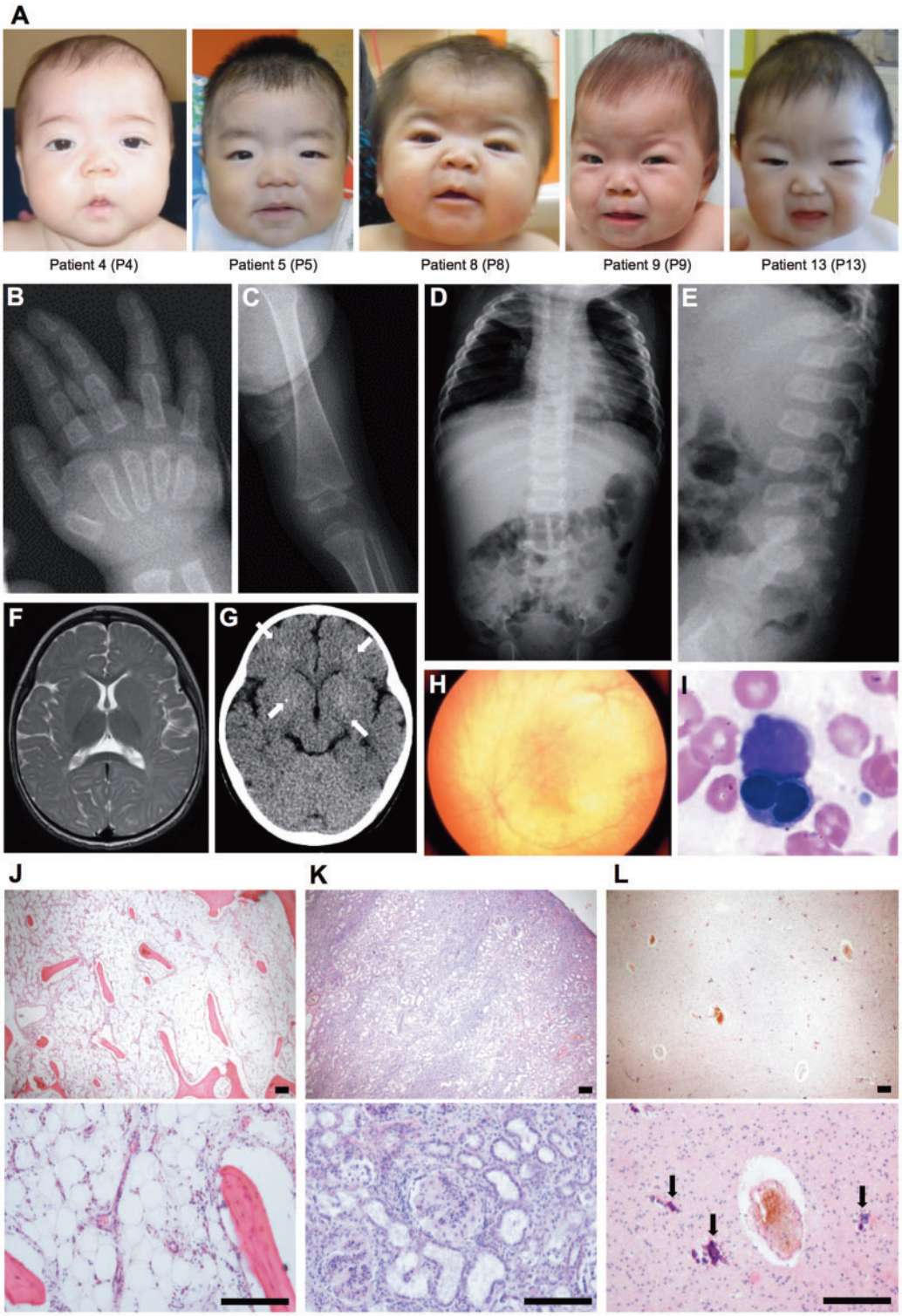

Figure 1. Clinical features of the patients. (**A**) Facial phenotypes. Patients have a prominent forehead, epicanthal folds, telecanthus, large rounded cheeks, broad nose, full lips, and short neck. The patient numbers correlate with the family pedigrees of Fig. 2A. (**B-I**) Findings of P9 at 11 months. (**B-E**) Radiographs showing the characteristic features of dysostosis multiplex. Note the bullet-shaped phalanges and the metacarpal pointing (**B**), metaphyseal widening of the long bones with cortical thinning (**C**), oar-shaped ribs (narrow at the vertebrae and widening anteriorly), flared iliac wings, and remarkable hepatomegaly (**D**), and malalignment of vertebrae and vertebral dysplasia with round vertebral bodies (**E**). (**F**) T2-weighted image of brain MRI showing apparent delayed myelination in the peripheral white matter. (**G**) Brain CT scan showing fine calcification in the basal ganglia and white matter (arrows). (**H**) Fundus photograph showing hypopigmentation of the retina. (**I**) Morphologic dysplasia of the erythroid lineage observed in the bone marrow. (**J-L**) Autopsy findings of P1 at 16 months. (**J**) Hypoplastic bone marrow in the sternum. (**K**) A significant grade of glomerular hyalinization and accumulation of lymphocytes in the renal interstitium. (**L**) Calcification in the cerebral white matter (arrows). Tissues were stained with hematoxylin and eosin. Scale bars, 200 μm. Consent to publish images of the patients was obtained.

Table 1. Clinical characteristics of the patients

Patient	P1	P2	P3	P4	P5	P6	P7	P8	P9	P10	P11	P12	P13
Sex	M	F	F	F	M	F	M	F	F	F	F	M	M
Age of death (months)(age at last observation)	30	20	10	17	19	12	35	20	Alive (11)	19	9	40	Alive (14)
MPS-like phenotype													
Coarse facial features	+	+	+	+	+	+	+	+	+	+	+	+	+
Joint contraction	+	+	+	+	+	+	+	+	+	+	+	+	+
Dysostosis multiplex (X-ray)	+	+	+	+	+	+	+	+	+	+	+	+	+
Hepatosplenomegaly	+	+	+	+	+	+	+	+	+	+	+	+	+
Respiratory disturbance	+	+	+	+	+	+	+	+	+	+	+	+	+
Psychomotor retardation	+	+	+	+	+	+	+	+	+	+	+	+	+
Able to walk	−	−	−	+	−	−	+	−	−	−	−	+	−
Able to speak words	−	−	−	−	−	−	−	−	−	−	−	−	−
Able to smile for family	+	+	+	+	+	+	+	+	+	+	+	+	+
Uncommon phenotypes for MPS													
Delayed myelination (MRI)	+	NA	NA	NA	NA	NA	NA	NA	+	+	NA	−	−
Brain atrophy (MRI)	+	NA	NA	NA	NA	NA	NA	NA	−	+	NA	−	−
Optic atrophy (Funduscopy)	+	+	+	+	+	−	+	−	−	−	−	−	−
Heart failure	+	+	+	+	+	+	+	+	−	+	+	+	−
Hypertrophic cardiomyopathy	+	+	+	+	+	+	+	−	−	+	+	−	−
Congenital heart defect (CHD)	PDA	PDA	ASD	ASD	ASD	PDA ASD	ASD	PDA	−	PDA	ASD	ASD	PDA
Surgery for CHD	−	+	−	+	−	+	−	−	−	+	−	−	−
Frequent respiratory infections	+	+	+	+	+	+	+	+	+	+	+	+	+
Anemia	+	+	+	+	+	+	+	+	+	+	+	+	+
Thrombocytopenia	+	+	+	+	+	+	+	+	−	+	+	+	+
Leukocytopenia	+	+	+	+	+	+	−	+	−	−	−	+	−
Bone marrow hypoplasia	+	NA	NA	NA	NA	NA	NA	NA	−	+	NA	NA	NA
Nephromegaly	+	−	+	−	+	−	−	−	−	−	−	−	−
Proteinuria	+	+	+	+	+	+	+	+	+	+	+	+	+
Nephritic syndrome	+	−	+	−	+	+	−	−	−	−	−	−	−

+, present; −, absent; F, female; M, male; m, months; NA, not available; PDA, patent ductus arteriosus; ASD, atrial septal defect.

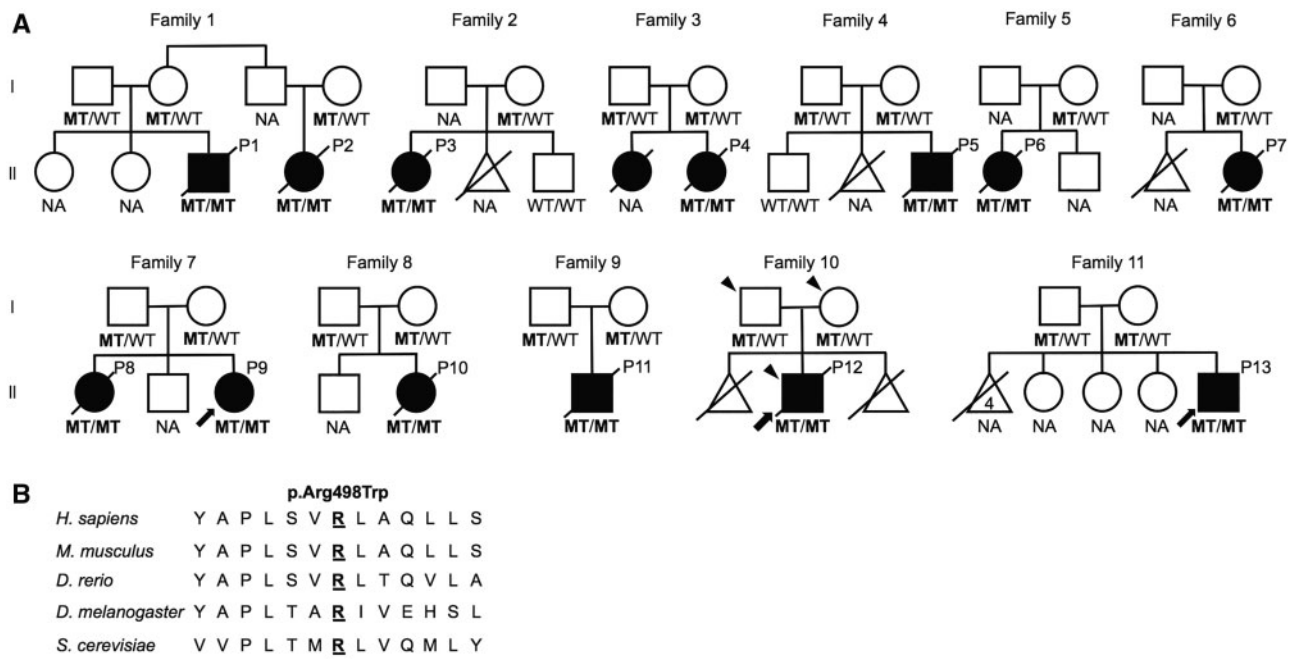

Figure 2. Family pedigrees and mutation analysis. (**A**) Pedigrees of the 11 families, indicating autosomal recessive inheritance. Affected individuals are shown in black. An affected sister of P4 had similar symptoms but was not available for gene testing. All affected individuals whose DNA was available were found to be homozygous for the c.1492C > T (p.R498W) mutation in *VPS33A* and their parents were heterozygous for the mutation. The individuals selected for exome sequencing are marked with an arrowhead. Arrows indicate individuals whose fibroblasts were analysed in this study. NA, not available; WT, wild-type allele; MT, mutant allele, c.1492C > T, p.R498W in *VPS33A*. (B) Amino acid alignment of VPS33A showing high conservation of the Arg498 residue among species.

of GAG, in plasma of patients, dermal fibroblasts from 3 patients (P9, P12, and P13; Fig. 2A), and VPS33A siRNA-treated HeLa cells. Plasma GAG levels are not routinely measured in MPS patients, but have recently been utilized for newborn screening (13). HS levels in patients' plasma were extremely high (301.1 and 412.2 μg/ml) compared with an MPS type II patient (60.6 μg/ml) and the normal reference range (5.1 ± 2.0 μg/ml) (Fig. 3A) (14). HS was also accumulated in patient-derived fibroblasts (Fig. 3B) and VPS33A-knockdown HeLa cells (Fig. 3C). These results suggested that VPS33A contributes to HS metabolism, and its dysfunction leads to HS accumulation and causes MPS-like phenotypes in humans.

To clarify the mechanisms of HS accumulation, we next investigated lysosomal functions in these cells. Lysosomal glycosidase activities in cell lysates, some of which contribute to GAG degradation, were not decreased in patient-derived fibroblasts (Supplementary Material, Fig. S2A). The colocalization of lysosomal enzymes and HS with lysosomal membrane markers indicates normal intracellular trafficking in patient-derived fibroblasts (Supplementary Material, Fig. S2B). Cathepsin D processing (Supplementary Material, Fig. S2C and D) and lipid trafficking (Supplementary Material, Fig. S2E) were not affected in patient-derived fibroblasts. However, LysoTracker signal intensity was increased in patient-derived fibroblasts and VPS33A-knockdown HeLa cells compared with normal controls (Fig. 3D and E). Since LysoTracker dye accumulates in acidic compartments, such as lysosomes, increased LysoTracker signal intensity suggests higher acidity (*i.e.* lower pH) of lysosomes. We hence directly measured lysosomal pH values in fibroblasts and VPS33A-knockdown HeLa cells. Lysosomal pH values were 4.92 ± 0.24 in control fibroblasts, 4.32 ± 0.20 in patient-derived fibroblasts, 5.41 ± 0.16 in Control siRNA-treated HeLa cells, and 4.98 ± 0.05 in VPS33A-knockdown HeLa cells (Fig. 3F). Therefore, lysosomal over-acidification was confirmed in patient-derived fibroblasts and VPS33A-depleted cells.

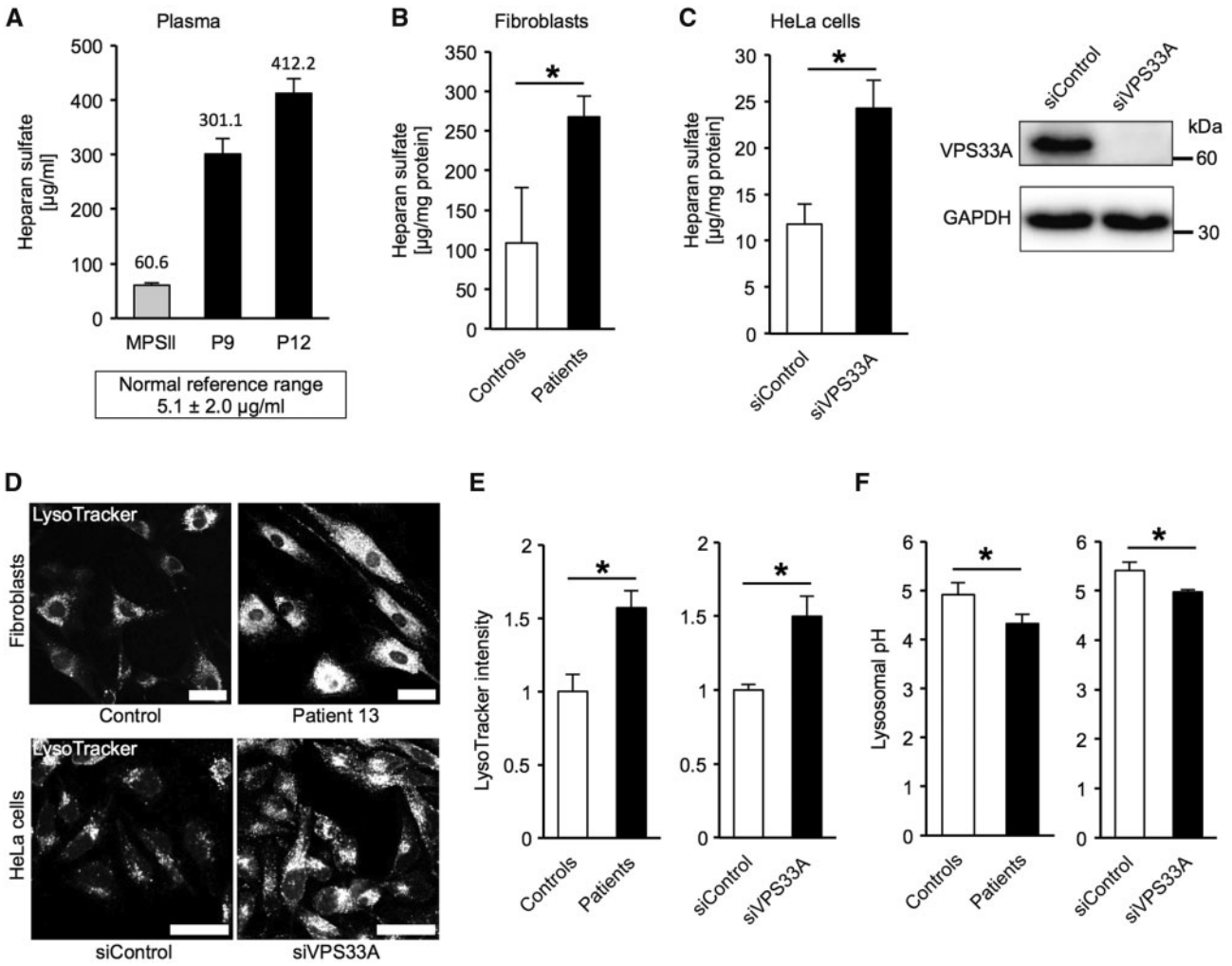

Figure 3. Quantification of heparan sulfate (HS) levels and lysosomal function. (**A-C**) HS quantification. (**A**) Plasma HS was accumulated in patients compared with an age-matched MPS patient and the reference range, which is 3.1 ± 2.0 (Mean ± SD) μg/ml (14). (**B**) HS accumulation in patient-derived fibroblasts and (**C**) VPS33A-knockdown HeLa cells. A western blot demonstrating the efficiency of knockdown of VPS33A is shown at the right. (**D-F**) Over-acidification of lysosomes in patient-derived fibroblasts and VPS33A-knockdown HeLa cells. (**D**) Patient-derived fibroblasts and VPS33A-knockdown HeLa cells showed increased intensities of LysoTracker compared to controls. (**E**) Quantification of LysoTracker intensity. LysoTracker intensities in LAMP2-positive areas were measured and relative levels to the control are shown. (**F**) Measurement of lysosomal pH in cells using LysoSensor Yellow/Blue DND-160. siVPS33A, HeLa cells treated with siRNA against VPS33A; siControl, siRNA of a negative-control sequence. Data are indicated as Mean and SEM (A) or SD (B, C, E and F) from 3 independent samples; *$P < 0.05$; Scale bars, 20 μm.

Analysis of domain-specific function of VPS33A

To examine whether the p.R498W mutation affects endocytic and autophagic pathways, we analysed patient-derived fibroblasts and VPS33A-knockdown HeLa cells. Cell surface epidermal growth factor receptor (EGFR) is internalized after EGF stimulation and is degraded in lysosomes through conventional endocytic degradation pathway (15,16). EGFR degradation was normal in patient-derived fibroblasts (Fig. 4A and Supplementary Material, Fig. S3A), indicating normal endocytic degradation activity. We then investigated the autophagic pathway, including autophagosome-lysosome fusion and degradation. To visualize autophagosome-lysosome fusion, we utilized the exogenous expression of mRFP-GFP (tandem fluorescent)-tagged LC3 (17), which localizes to autophagosome membranes (18). Autophagosomes initially exhibit both GFP and mRFP fluorescence. When autophagosomes are fused with lysosomes and mature into acidic autolysosomes, these autolysosomes have reduced GFP signals but maintain their mRFP signals. We observed no differences in the autophagosomes: autolysosomes ratio between patient-derived fibroblasts and controls (Supplementary Material, Fig. S4), suggesting normal autophagosome-lysosome fusion in patient-derived fibroblasts. Total autophagic degradation activity was estimated by the amount of LC3-II turnover using immunoblotting. Incubating cells with the lysosomal inhibitor bafilomycin A1 causes the accumulation of undegraded LC3-II, which corresponds to autophagic flux. Autophagic flux was blocked in VPS33A-knockdown HeLa cells, as previously reported (7) (Fig. 4B). However, autophagic flux was normal in patient-derived fibroblasts (Fig. 4B, Supplementary Material, Fig. S3B and C). These results indicate that patient-derived fibroblasts have normal endocytic and autophagic function.

VPS33A was reported to bind to VPS16 within the HOPS complex (Fig. 4C) (19). VPS33A was also reported to bind to syntaxin 17 (STX17; an autophagosomal SNARE), and to mediate autophagosome-lysosome fusion (5,7). To investigate the interaction between mutant VPS33A (p.R498W), VPS16, and STX17, we expressed human HA-tagged VPS33A (wild-type and mutant) together with Myc-tagged VPS16 or FLAG-tagged STX17 in HEK 293T cells, and immunoprecipitated these proteins with anti-HA or anti-FLAG antibodies. The interaction of mutant VPS33A, VPS16, and STX17 was not altered compared with the wild-type protein (Fig. 4E and F). The p.R498W mutation is hence unlikely to affect these protein interactions.

Discussion

The HOPS complex is a large multisubunit tethering complex that binds organelles together and regulates late endosome-lysosome and autophagosome-lysosome fusion (2–7). The complex comprises six subunits (VPS11, VPS16, VPS18, VPS33A, VPS39, and VPS41). Knockdown of their genes affects endocytic and autophagic pathways (5–7). The VPS33A protein comprises 4 domains: 1, 2, 3a, and 3b (Fig. 4D) (20,21). VPS33A binds only to VPS16 within the complex, and domain 3b of VPS33A is the binding interface to VPS16 (20). The fusion of lysosomes with endosomes or autophagosomes is affected in HeLa cells with mutation in domain 3b of VPS33A, which no longer bind with VPS16 (6). These facts indicate that the binding between VPS33A and VPS16 is crucial for the function of the entire HOPS complex including the fusion of lysosomes with endosomes or autophagosomes. VPS33A is also a member of SM proteins which comprise, together with SNAREs, the core machinery essential for membrane fusion (22). VPS33A binds to STX17 (an autophagosomal SNARE), and the HOPS complex mediates autophagosome-lysosome fusion through interaction with STX17 (5,7). Knockdown of STX17 affects the autophagic pathway, but not the endocytic pathway. Domain 3a of VPS33A is predicted to be the interacting interface to the SNARE complex (21). The Arg498 residue is located in domain 2, which is thought not to interact with VPS16 nor the SNARE complex (Fig. 4D) (20,21). Indeed, we showed that the p.R498W mutation did not affect these protein interactions. This might be the reason why neither endocytic nor autophagic pathways were affected in patient-derived fibroblasts, in contrast to VPS33A-depleted cells. The p.Asp251Glu mutation seen in the murine *Vps33a* mutant mouse, *buff* mouse, is located in domain 3a, and affects autophagosome-lysosome fusion without disrupting endosome-lysosome fusion (23), which further supports our hypothesis.

Homologs of HOPS components can be identified in almost all eukaryotic genomes (24) and are thought to be essential; for example, removal of the *VPS33A* homolog *carnation* in *Drosophila* causes a lethal outcome during larval development (2). A disease-causing mutation in the *VPS33A* gene has never been reported in humans to date. The mouse with a missense mutation (p.Asp251Glu: *Vps33a*^{bf}), *buff* mouse, exhibits hypopigmentation and decreased platelet activity, resembling the phenotype of Hermansky-Pudlak syndrome (HPS) in humans (25). However, our patients showed an MPS-like phenotype, and characteristic symptoms of HPS, such as cutaneous albinism and bleeding diathesis were not observed. Hypopigmentation in the retina observed in patient 9 (Fig. 1H) was the only phenotype common with the *buff* mouse. Our results therefore suggest that the different domains within the VPS33A protein are responsible for its different functions.

MPS represents the largest group of lysosomal storage disorders (LSDs) and are characterized by progressive multiple organ involvement, leading to severe disability and premature death (1). Each type of MPS results from a deficiency of a specific lysosomal enzyme that participates in the stepwise degradation of GAG. Although our patients showed typical manifestations of MPS and increased secretion of urinary GAG, lysosomal enzyme activities involved in GAG degradation were not decreased (Supplementary Materials, Table S1 and Fig. S2A). The results of exome sequencing of patient 12 showed no pathogenic mutation in the known genes of conventional MPS (data not shown). To confirm the association between the p.R498W mutation of VPS33A and GAG accumulation, we investigated the level of HS in patient-derived fibroblasts and VPS33A-depleted cells. Both of these cells showed HS accumulation, suggesting that this mutation was associated with GAG accumulation. Although the extremely high concentrations of plasma HS in our patients suggested that this mutation affects the intracellular uptake or trafficking of GAG, intracellular trafficking in patient-derived fibroblasts was normal (Supplementary Material, Fig. S2B). We also demonstrated lysosomal over-acidification in patient-derived fibroblasts and VPS33A-depleted cells by lysosomal function analysis. The increased LysoTracker signal in VPS33A-depleted cells has already been reported in the literature, but its significance has not been clarified (7). Because lysosomal enzyme activities of glycosidases were measured in cell lysates in an optimal pH buffer (Supplementary Material, Fig. S2A), they may not reflect the *in vivo* degradative function of glycosidases. Some studies suggested that the over-acidified environment within lysosomes resulted in the malfunction of various lysosomal

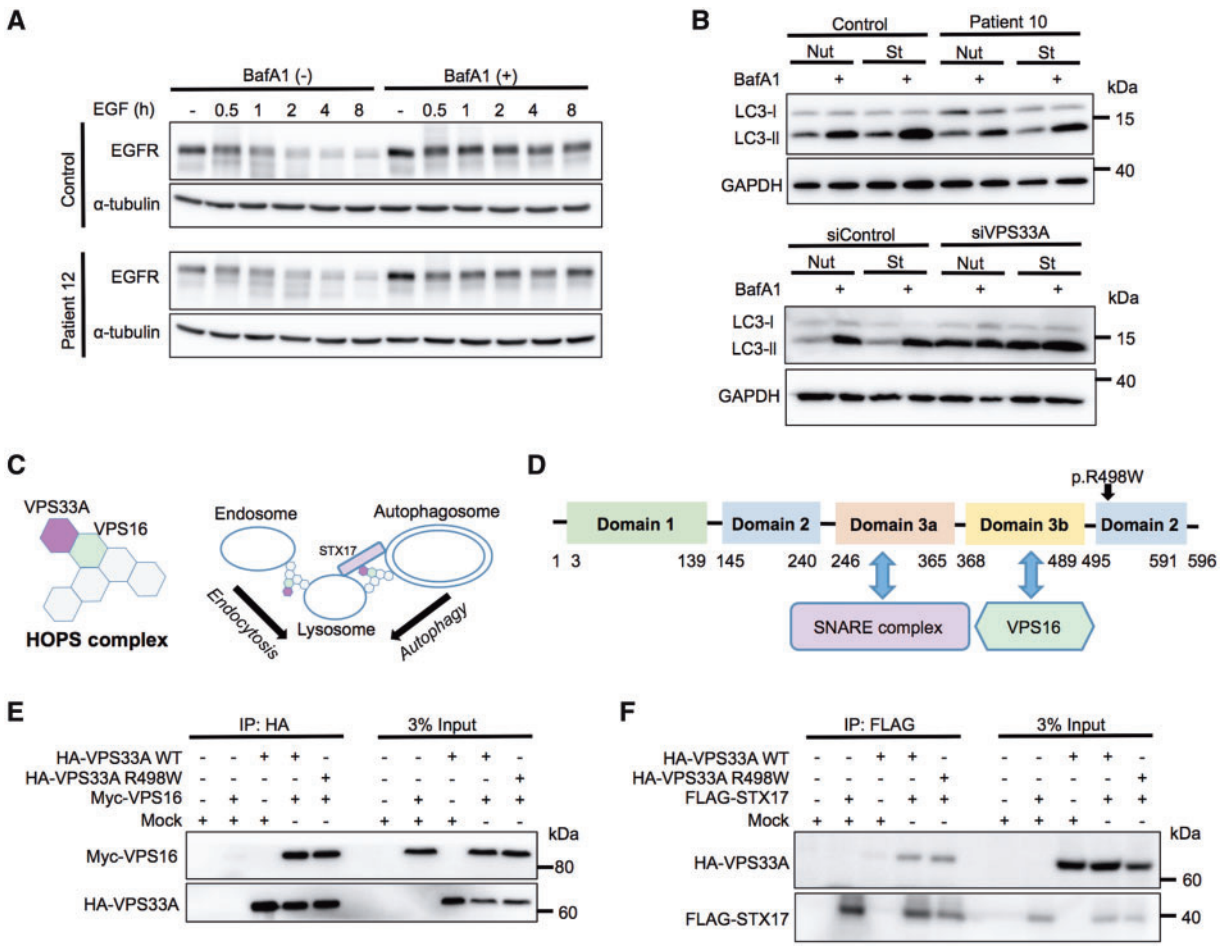

Figure 4. Endocytic and autophagic functions in fibroblasts and interactions of mutant VPS33A with STX17 or VPS16. (**A**) Immunoblot analysis showing normal EGFR degradation in patient-derived fibroblasts. Cells were treated with bafilomycin A1 (BafA1, 125 nM) as a negative control of degradation, and stimulated with 100 ng/ml EGF at time 0. Samples were analysed by immunoblotting at the indicated time points. (**B**) Normal autophagic flux in patient-derived fibroblasts (upper), in contrast to VPS33A-knockdown HeLa cells (lower). Cells were treated with regular or starvation medium for 2 h with or without BafA1, and analysed by immunoblotting. Nut, nutrient-rich condition; St, starved condition. Quantifications of A and B are shown in Supplementary Material, Fig. S3A–C. (**C**) Schematic model of the human HOPS complex (left), and its interaction with STX17 (an autophagosomal SNARE) or organelles (right); both modified from ref.6. (**D**) A diagram of the predicted VPS33A domains and their interaction partners. The p.R498W mutation detected in this report is located in domain 2, which has not been reported to interact with SNARE complex or VPS16. (**E,F**) Immunoprecipitation and immunoblot analysis of VPS33A, VPS16, and STX17. (E) HA-VPS33A (wild-type (WT) or mutant) and Myc-VPS16 were cotransfected in HEK293T cells. Cells were lysed, immunoprecipitated with an anti-HA-agarose antibody, and analysed by immunoblotting. (F) HA-VPS33A (WT or mutant) and FLAG-STX17 were cotransfected in HEK293T cells. Cells were lysed, immunoprecipitated with an anti-FLAG M2 affinity gel, and analysed by immunoblotting. The results indicate that the p.R498W mutant of VPS33A can interact with both VPS16 and STX17. siVPS33A, HeLa cells treated with siRNA against VPS33A; siControl, siRNA of a negative-control sequence; IP, immunoprecipitation.

hydrolases, leading to a substrate accumulation in mucolipidosis type lV (MLIV), one of LSDs (26,27), and HS is indeed accumulated in MLIV fibroblasts (28). In the MLIV, lysosomal accumulation of undegraded substrates was cleared by the treatment with H+/K+ ionophore (Nigericin) or a weak base (Chloroquine) that correct over-acidification of lysosomes. They concluded that over-acidification of lysosomes causes lysosomal dysfunction and storage of undegraded substrates (26,27). Thus, we speculate that lysosomal over-acidification might be associated with GAG accumulation and contribute to MPS-like phenotypes in our patients. Recently, *VPS11* mutations in patients with infantile onset leukoencephalopathy were reported (29–31). The patients presented with primary and severe developmental delay associated with variable seizures, spastic tetraplegia, truncal hypotonia, cortical blindness, hearing loss, and microcephaly. These clinical phenotypes are different from those of our patients. Interestingly, however, the patients with *VPS11* mutations showed distinct lysosomal storage phenomena and increased urinary levels of glycosphingolipids, suggesting that the defect of a component of the HOPS complex causes accumulation of lysosomal substrates without lysosomal enzyme defects. These reports support our data that a defect of VPS33A, a component of the HOPS complex, causes GAG accumulation.

In conclusion, we report a novel disease of impaired GAG metabolism caused by a specific mutation in the *VPS33A* gene in the Yakut population. Although the detailed mechanism and disease pathophysiology, as well as the domain-specific function of VPS33A remain to be elucidated, our results indicate a new function of VPS33A: the regulation of lysosomal acidification and GAG metabolism other than in endocytosis or autophagy. Clinical phenotypes of this disease are similar to conventional MPS caused by enzymatic deficiencies of GAG metabolism, and this disease should hence be considered as a differential diagnosis for MPS.

Materials and Methods

Subjects

Informed consent was obtained from all subjects or their parents. The Institutional Review Board of Osaka University approved the study. DNA samples of 110 healthy Yakut controls were obtained from Bank of the Laboratory of Genome Medicine of Clinics of North East Federal University.

Whole exome capture and sequencing

For every subject in the family, the sequence reads were converted using perl scripts from Illumina fastq format to fastq files that conform to the Sanger specification for base-quality encoding. Burroughs Wheeler Alignment (BWA) version 0.7.10 was used to align the sequencing reads, and default parameters were used for fragment reads, to the human reference sequence (hg19) (32). Alignments were converted from SAM format to sorted and indexed BAM files with SamTools. The Picard-tools were used to remove invalid alignments and duplicate reads from the BAM files. Regions surrounding potential indels were realigned with the GATK 2.5-2 IndelRealigner (33).

Genotypes were called with the GATK 2.5-2 UnifiedGenotyper. We then analysed the union of single nucleotide variant (SNV) and indel variant calls from GATK with the ANNOVAR program to identify exonic or splicing variants with their allele frequency and functional annotation (34). We analysed the location and genotype of variants for each individual to locate the subset of variants on the autosomal chromosome. All variant calls present on the X and Y chromosome were removed given the mode of inheritance of the disease. Variants with either quality scores below 50, a read depth of less than 5, or a QUAL score normalized by allele depth (QD) below 1.5 were filtered out. Output files from GATK were in VCF format.

All variants were annotated with the ANNOVAR program with respect to their frequency in the 1000 Genomes Project, NHLBI Exome Sequencing Project (ESP), and Exome Aggregation Consortium (ExAC). Impact on coding features were analysed using perl scripts against the following 3 databases: refGene tracks from the NCBI Reference Sequence Database, knownGene tracks from the UCSC Known Genes, and ensGene tracks from Ensemble Genes (34,35). We assumed a homozygous mutation owing to autosomal recessive inheritance in the family. We selected candidate variants with the following criteria; 1) either an exonic or splice site in at least 1 database; 2) either nonsynonymous, splice site, insertion/deletion, stop gain/loss, or unknown variants in at least 1 database; 3) PASS in GATK annotation; 4) a minor allele frequency of less than 0.1% in the total population in 1000 Genomes Project or ESP6500, or in the East Asian population in ExAC.

Verification of the p.R498W mutation in the *VPS33A* gene was confirmed by Sanger sequencing using 5'-AGGGGTGGG GGTTGTATATC-3' and 5'-GCAACTGTACAATACCTGAAAACC-3' primers.

Cell culture and RNA interference

Dermal fibroblasts were established from three patients. Three normal human dermal fibroblast cell lines were purchased (Lonza, Invitrogen, and Gibco). Fibroblasts were cultured in Dulbecco's Modified Eagle Medium (DMEM) supplemented with 10% heat inactivated fetal bovine serum (FBS) and antibiotic-antimycotic solution (referred to as regular medium) in a 5% CO_2 incubator. Silencer Select RNA interference oligonucleotides were used for siRNA experiments (Life Technologies). Silencer Select Negative Control No. 1 siRNA (4390843, Life Technologies) and human VPS33A siRNA antisense (s35197, Life Technologies) were used. The siRNA oligonucleotides were transfected into cells using Lipofectamine RNAi MAX (Life Technologies). After 2 days, cells were again transfected with the same siRNA and cultured for an additional 2 days before analysis.

Antibodies

Primary antibodies used were horseradish peroxidase (HRP)-conjugated anti-GAPDH (M171-7, MBL), anti-EGFR (MI-12-1, MBL), anti-α-tubulin (T5168, Sigma), anti-LC3 (PM036, MBL), HRP-conjugated anti-HA (clone 3F10, Roche), HRP-conjugated anti-FLAG (A8592, Sigma), HRP-conjugated anti-Myc (ab1261, Abcam), anti-LIMP2 (NB400-129, NOVUS), anti-heparan sulphate (clone 10E4, Seikagaku Biobusiness), anti-LAMP2 (clone H4B4, Santa Cruz Biotechnology), anti-α-L-iduronidase (AF4119, R&D Systems), anti-cathepsin B (sc6493, Santa Cruz Biotechnology), and anti-cathepsin D (sc6468, Santa Cruz Biotechnology). Secondary antibodies used were HRP-conjugated anti-rabbit immunoglobulin G (IgG) (NA934, GE Healthcare), Alexa 488-conjugated anti-mouse (R37114, Invitrogen), Alexa 488-conjugated anti-sheep IgG (A-11015, Invitrogen), Alexa 555-conjugated anti-mouse IgG A-31570, Invitrogen), and Alexa 647-conjugated anti-rabbit IgG (ab150075, Abcam).

Immunoprecipitation and immunoblotting

HEK 293T cells were transiently transfected using Lipofectamine 2000 reagent (Invitrogen) with the indicated plasmids. The next day, cells were collected by scraping in lysis buffer containing CHAPS (30 mM 3-morpholinopropanesulfonate, pH 8, 150 mM NaCl, 1 mM EDTA, 10% glycerol, 1% 3-[(3-cholamidopropyl) dimethylammonio]-1-propanesulfonate, a phosphatase inhibitor cocktail (PhosSTOP Phosphatase Inhibitor Cocktail, Roche), and a protease inhibitor cocktail (Complete EDTA-free protease inhibitor, Roche). Cell lysates were clarified by centrifugation at 21,000 × *g*, and precleared with IgG agarose beads (A0919, Sigma). Precleared lysates were subjected to immunoprecipitation with anti-FLAG M2 affinity gel (A2220, Sigma), or a monoclonal anti-HA-agarose antibody (A2095, Sigma). The immunoprecipitated complexes were washed 3 times in lysis buffer. Samples were subsequently separated by SDS–PAGE and transferred to PVDF membranes (GE Healthcare). Immunoblot analysis was performed and visualized with ECL Western Blotting Analysis System (RPN2109, GE Healthcare) or Lumina Forte Western HRP Substrate (WBLUF0100, Millipore).

EGFR degradation assay

Cells were cultured in regular medium to approximately 70% confluency, washed twice with warm serum-free DMEM, and incubated in serum-free DMEM from -2 h. Bafilomycin A1 (BafA1, B-1080, LC Laboratories) was added to the medium (125 nM) at -1 h, and EGF (53003018, Thermo Fisher Scientific) was added to the medium (100 ng/ml) at time 0. Cells were washed once with PBS, collected, and lysed at the indicated time points. Samples were subsequently lysed and analysed by immunoblotting.

Assays for autophagy

Cells were transfected with mRFP-GFP-LC3 for 48 h and then incubated with regular medium (nutrient-rich condition) or Earle's Balanced Salt Solution (EBSS) (starved condition) for 2 h. Then, cells were fixed and their GFP and mRFP fluorescence was analysed by microscopy (17). For autophagic flux analysis, cells were plated and cultured in regular medium one day before the assay. At the time of the assay, the cells were approximately 70% confluent. Cells were washed twice with warm PBS and incubated in regular medium or EBSS with or without 125 nM BafA1. After 2 h, cells were washed with PBS, collected, and lysed. Samples were subsequently subjected to immunoblotting to detect LC3 and GAPDH. The amount of membrane-bound LC3-II was quantitated as an indicator of autophagic vacuoles, and the differences in LC3-II intensities between the presence and absence of BafA1 represent autophagic degradation activities (flux) during the assay period (2 h).

Expression vectors

FLAG-Stx17 was a gift from Noboru Mizushima (Addgene plasmid #45911). The wild-type VPS33A expression vector was provided by RIKEN BRC through the National Bio-Resource Project of the MEXT, Japan. We constructed the HA-tagged VPS33A (wild-type (WT) and mutant) expression vectors and the Myc-tagged VPS16 expression vector. All constructs were verified by DNA sequencing.

Heparan sulphate measurement

Amounts of HS in patients' plasma and fibroblast lysate, or siRNA-treated HeLa cell lysate were measured according to the manufacturer's protocol (HS-ELISA Kit, Seikagaku Biobusiness). Amounts of HS were calculated as μg HS/mg protein or μg HS/ml.

Lysosomal enzyme activity assay

Activities of lysosomal enzymes were measured with artificial 4-methylumbelliferyl (4-MU) substrates (M3657, M8527, M9766, M3633, and M1633, Sigma; 474422 and 474525, Calbiochem; 44009, Glycosynth; 2340-34, Nacalai) (36). Cells were collected in water, sonicated, and their protein concentrations were determined by the Lowry method (37). The samples were incubated with specific 4-MU substrates in acidic phosphate or citrate buffer at 37 °C for 1 h, and the fluorescence upon excitation at 365 nm/emission at 450 nm was measured using a microplate reader (SH9000Lab, Corona). A 4-MU standard (M1381, Sigma) was also measured in the same buffer to calculate enzyme activities as nmol/h/mg of protein.

Immunocytochemistry and filipin staining

Cells grown on coverslips were washed with PBS and fixed in 4% paraformaldehyde in PBS for 10 min at room temperature. The fixed cells were permeabilized with 50 μg/ml digitonin in PBS for 10 min, blocked with 3% bovine serum albumin in PBS for 1 h, and incubated with primary antibodies for 1 h. After washing with PBS, cells were incubated with fluorescence-conjugated secondary antibodies for another 1 h. For filipin staining, fixed cells were permeabilized with 0.1% Triton-X in PBS for 15 min, and incubated in the dark with 300 μg/ml filipin complex (F9765, Sigma) in PBS for 8 h. Control fibroblasts were also treated with 5 μM U18666A (U3633, Sigma) for 24 h to accumulate free cholesterol, and was used as a positive control. Images were acquired on a confocal laser-scanning microscope or a wide field fluorescence microscope (Olympus).

Measurement of lysosomal acidity

Cells were plated onto clear-bottom 96-well plates (Greiner) and stained with 100 nM LysoTracker Red DND-99 (L-7518, Molecular Probes) for 1 h. The cells were then fixed and stained for LAMP2 as described above, together with Hoechst 33258 (H341, Dojindo) and HCS CellMask Stains (H32721, Molecular Probes). Samples were analysed by automated epifluorescence microscopy (IN Cell Analyzer 2000, GE Healthcare). In brief, areas of cells were identified by HCS CellMask Stains, and the mean intensity of LysoTracker in LAMP2-positive areas were quantified.

Quantification of lysosomal pH was performed using the ratiometric lysosomal pH dye LysoSensor Yellow/Blue DND-160 (L7545, Molecular Probes). Cells were plated in 96-well plates and labelled with 5 μM LysoSensor Yellow/Blue DND-160 for 5 min at room temperature, and excessive dye was washed out using PBS. The fluorescence of labelled cells was measured in MES buffer (5 mM NaCl, 115 mM KCl, 1.3 mM MgSO4, 25 mM MES, pH 7.0). The standard curve was generated by incubating cells in 10 μM monensin (22373-78-0, LKT Laboratories) and 10 μM Nigericin (28463-80-3, LKT Laboratories) in MES buffer (pH 4.0–6.0). Samples were then read using a microplate reader (SH9000Lab, Corona) at excitation 365 nm/emission 450 nm and excitation 385 nm/emission 550 nm. The pH values were determined from the standard curve generated using the pH calibration samples (38,39).

Statistical analysis

Numerical data are presented as the Mean and SEM or SD. The distribution of values was tested by the *F*-test. For testing significant differences between samples, the unpaired Student's *t*-test was used.

Web Resources

The URLs for data presented herein are as follows: VCF, https://samtools.github.io/hts-specs/VCFv4.1.pdf; date last accessed March 2015; 1000 Genomes Project, http://www.1000genomes.org/; date last accessed March 2015; ESP6500, http://evs.gs.washington.edu/EVS/; date last accessed March 2015; ExAC, http://exac.broadinstitute.org/; date last accessed March 2015.

Supplementary Material

Supplementary Material is available at *HMG* online.

Acknowledgements

We thank the subjects and their families for their participation in this study. We thank K. Tsujimoto (Osaka University) for technical assistance, and T. Endo (Osaka University) for fundus examination. We thank T. Kubota, T. Kitaoka, S. Nabatame, T. Miyamura, and J. Tanigawa (Osaka University) for fruitful discussions. We are grateful to the Center for Medical Research and Education, and the Center of Medical Innovation and Translational Research, Graduate School of Medicine, Osaka University, for technical support.

Conflict of Interest statement. None declared.

Funding

This work was supported by the Practical Research Project for Rare/Intractable Diseases (16ek0109151h0002) from the Japan Agency for Medical Research and Development (AMED) and the Grant-in-Aid for Scientific Research (KAKENHI) (C:25461543, 15H05673) from the Japan Society for the Promotion of Science (JSPS).

References

1. Neufeld, E.F. M.J. The Mucopolysaccharidoses. *The Online Metabolic and Molecular Bases of Inherited Disease*, http://ommbid.mhmedical.com/book.aspx?bookid=971; date last accessed October, 2016.
2. Akbar, M.A., Ray, S. and Kramer, H. (2009) The SM protein Car/Vps33A regulates SNARE-mediated trafficking to lysosomes and lysosome-related organelles. *Mol. Biol. Cell*, **20**, 1705–1714.
3. Lobingier, B.T. and Merz, A.J. (2012) Sec1/Munc18 protein Vps33 binds to SNARE domains and the quaternary SNARE complex. *Mol. Biol. Cell*, **23**, 4611–4622.
4. Balderhaar, H.J. and Ungermann, C. (2013) CORVET and HOPS tethering complexes - coordinators of endosome and lysosome fusion. *J. Cell. Sci.*, **126**, 1307–1316.
5. Takats, S., Pircs, K., Nagy, P., Varga, A., Karpati, M., Hegedus, K., Kramer, H., Kovacs, A.L., Sass, M. and Juhasz, G. (2014) Interaction of the HOPS complex with Syntaxin 17 mediates autophagosome clearance in Drosophila. *Mol. Biol. Cell*, **25**, 1338–1354.
6. Wartosch, L., Gunesdogan, U., Graham, S.C. and Paul Luzio, J. (2015) Recruitment of VPS33A to HOPS by VPS16 is required for lysosome fusion with endosomes and autophagosomes. *Traffic*, **16**, 727–742.
7. Jiang, P., Nishimura, T., Sakamaki, Y., Itakura, E., Hatta, T., Natsume, T. and Mizushima, N. (2014) The HOPS complex mediates autophagosome-lysosome fusion through interaction with syntaxin 17. *Mol. Biol. Cell*, **25**, 1327–1337.
8. Barashkov, N.A., Dzhemileva, L.U., Fedorova, S.A., Teryutin, F.M., Posukh, O.L., Fedotova, E.E., Lobov, S.L. and Khusnutdinova, E.K. (2011) Autosomal recessive deafness 1A (DFNB1A) in Yakut population isolate in Eastern Siberia: extensive accumulation of the splice site mutation IVS1+1G>A in GJB2 gene as a result of founder effect. *J. Hum. Genet.*, **56**, 631–639.
9. Pakendorf, B., Novgorodov, I.N., Osakovskij, V.L., Danilova, A.P., Protod'jakonov, A.P. and Stoneking, M. (2006) Investigating the effects of prehistoric migrations in Siberia: genetic variation and the origins of Yakuts. *Hum. Genet.*, **120**, 334–353.
10. Maksimova, N., Hara, K., Miyashia, A., Nikolaeva, I., Shiga, A., Nogovicina, A., Sukhomyasova, A., Argunov, V., Shvedova, A., Ikeuchi, T., *et al.* (2007) Clinical, molecular and histopathological features of short stature syndrome with novel CUL7 mutation in Yakuts: new population isolate in Asia. *J. Med. Genet.*, **44**, 772–778.
11. Maksimova, N., Hara, K., Nikolaeva, I., Chun-Feng, T., Usui, T., Takagi, M., Nishihira, Y., Miyashita, A., Fujiwara, H., Oyama, T., *et al.* (2010) Neuroblastoma amplified sequence gene is associated with a novel short stature syndrome characterised by optic nerve atrophy and Pelger-Huet anomaly. *J. Med. Genet.*, **47**, 538–548.
12. Gormez, Z., Bakir-Gungor, B. and Sagiroglu, M.S. (2014) HomSI: a homozygous stretch identifier from next-generation sequencing data. *Bioinformatics*, **30**, 445–447.
13. Tomatsu, S., Fujii, T., Fukushi, M., Oguma, T., Shimada, T., Maeda, M., Kida, K., Shibata, Y., Futatsumori, H., Montano, A.M., *et al.* (2013) Newborn screening and diagnosis of mucopolysaccharidoses. *Mol. Genet. Metab.*, **110**, 42–53.
14. Tomatsu, S., Gutierrez, M.A., Ishimaru, T., Pena, O.M., Montano, A.M., Maeda, H., Velez-Castrillon, S., Nishioka, T., Fachel, A.A., Cooper, A., *et al.* (2005) Heparan sulfate levels in mucopolysaccharidoses and mucolipidoses. *J. Inherit. Metab. Dis.*, **28**, 743–757.
15. Carpenter, G. and Cohen, S. (1976) 125I-labeled human epidermal growth factor. Binding, internalization, and degradation in human fibroblasts. *J. Cell. Biol.*, **71**, 159–171.
16. Yoshimori, T., Yamamoto, A., Moriyama, Y., Futai, M. and Tashiro, Y. (1991) Bafilomycin A1, a specific inhibitor of vacuolar-type H(+)-ATPase, inhibits acidification and protein degradation in lysosomes of cultured cells. *J. Biol. Chem.*, **266**, 17707–17712.
17. Kimura, S., Noda, T. and Yoshimori, T. (2007) Dissection of the autophagosome maturation process by a novel reporter protein, tandem fluorescent-tagged LC3. *Autophagy*, **3**, 452–460.
18. Kabeya, Y., Mizushima, N., Ueno, T., Yamamoto, A., Kirisako, T., Noda, T., Kominami, E., Ohsumi, Y. and Yoshimori, T. (2000) LC3, a mammalian homologue of yeast Apg8p, is localized in autophagosome membranes after processing. *EMBO J.*, **19**, 5720–5728.
19. Galmes, R., Ten Brink, C., Oorschot, V., Veenendaal, T., Jonker, C., van der Sluijs, P. and Klumperman, J. (2015) Vps33B is required for delivery of endocytosed cargo to lysosomes. *Traffic*, **12**, 1288–1305.
20. Graham, S.C., Wartosch, L., Gray, S.R., Scourfield, E.J., Deane, J.E., Luzio, J.P. and Owen, D.J. (2013) Structural basis of Vps33A recruitment to the human HOPS complex by Vps16. *P. Natl. Acad. Sci. USA*, **110**, 13345–13350.
21. Baker, R.W., Jeffrey, P.D. and Hughson, F.M. (2013) Crystal Structures of the Sec1/Munc18 (SM) Protein Vps33, Alone and Bound to the Homotypic Fusion and Vacuolar Protein Sorting (HOPS) Subunit Vps16*. *PloS. One*, **8**, e67409.
22. Sudhof, T.C. and Rothman, J.E. (2009) Membrane fusion: grappling with SNARE and SM proteins. *Science*, **323**, 474–477.
23. Zhen, Y. and Li, W. (2015) Impairment of autophagosome-lysosome fusion in the buff mutant mice with the VPS33A(D251E) mutation. *Autophagy*, **11**, 1608–1622.
24. Koumandou, V.L., Dacks, J.B., Coulson, R.M. and Field, M.C. (2007) Control systems for membrane fusion in the ancestral eukaryote; evolution of tethering complexes and SM proteins. *BMC. Evol. Biol.*, **7**, 29.
25. Suzuki, T., Oiso, N., Gautam, R., Novak, E.K., Panthier, J.J., Suprabha, P.G., Vida, T., Swank, R.T. and Spritz, R.A. (2003) The mouse organellar biogenesis mutant buff results from a mutation in Vps33a, a homologue of yeast vps33 and Drosophila carnation. *P. Natl. Acad. Sci. USA*, **100**, 1146–1150.
26. Soyombo, A.A., Tjon-Kon-Sang, S., Rbaibi, Y., Bashllari, E., Bisceglia, J., Muallem, S. and Kiselyov, K. (2006) TRP-ML1 regulates lysosomal pH and acidic lysosomal lipid hydrolytic activity. *J. Biol. Chem.*, **281**, 7294–7301.
27. Kogot-Levin, A., Zeigler, M., Ornoy, A. and Bach, G. (2009) Mucolipidosis type IV: the effect of increased lysosomal pH on the abnormal lysosomal storage. *Pediatr. Res.*, **65**, 686–690.
28. Bach, G., Ziegler, M., Kohn, G. and Cohen, M.M. (1977) Mucopolysaccharide accumulation in cultured skin fibroblasts derived from patients with mucolipidosis IV. *Am. J. Hum. Genet.*, **29**, 610–618.

29. Edvardson, S., Gerhard, F., Jalas, C., Lachmann, J., Golan, D., Saada, A., Shaag, A., Ungermann, C. and Elpeleg, O. (2015) Hypomyelination and developmental delay associated with VPS11 mutation in Ashkenazi-Jewish patients. *J. Med. Genet.*, **52**, 749–753.
30. Zhang, J., Lachance, V., Schaffner, A., Li, X., Fedick, A., Kaye, L.E., Liao, J., Rosenfeld, J., Yachelevich, N., Chu, M.L., *et al.* (2016) A Founder Mutation in VPS11 Causes an Autosomal Recessive Leukoencephalopathy Linked to Autophagic Defects. *PLoS. Genet.*, **12**, e1005848.
31. Hortnagel, K., Krageloh-Mann, I., Bornemann, A., Docker, M., Biskup, S., Mayrhofer, H., Battke, F., du Bois, G. and Harzer, K. (2016) The second report of a new hypomyelinating disease due to a defect in the VPS11 gene discloses a massive lysosomal involvement. *J. Inherit. Metab. Dis.*, **39,** 849–857.
32. Li, H. and Durbin, R. (2009) Fast and accurate short read alignment with Burrows-Wheeler transform. *Bioinformatics*, **25**, 1754–1760.
33. McKenna, A., Hanna, M., Banks, E., Sivachenko, A., Cibulskis, K., Kernytsky, A., Garimella, K., Altshuler, D., Gabriel, S., Daly, M., *et al.* (2010) The Genome Analysis Toolkit: a MapReduce framework for analyzing next-generation DNA sequencing data. *Genome Res.*, **20**, 1297–1303.
34. Wang, K., Li, M. and Hakonarson, H. (2010) ANNOVAR: functional annotation of genetic variants from high-throughput sequencing data. *Nucleic. Acids. Res.*, **38**, e164.
35. Genomes Project, C., Abecasis, G.R., Auton, A., Brooks, L.D., DePristo, M.A., Durbin, R.M., Handsaker, R.E., Kang, H.M., Marth, G.T. and McVean, G.A. (2012) An integrated map of genetic variation from 1,092 human genomes. *Nature*, **491**, 56–65.
36. Hindman, J. and Cotlier, E. (1972) Glycosidases in normal human leukocytes and abnormalities in G M1 -gangliosidosis. *Clin. Chem.*, **18**, 971–975.
37. Lowry, O.H., Rosebrough, N.J., Farr, A.L. and Randall, R.J. (1951) Protein measurement with the Folin phenol reagent. *J. Biol. Chem.*, **193**, 265–275.
38. Wolfe, D.M., Lee, J.H., Kumar, A., Lee, S., Orenstein, S.J. and Nixon, R.A. (2013) Autophagy failure in Alzheimer's disease and the role of defective lysosomal acidification. *Eur. J. Neurosci.*, **37**, 1949–1961.
39. Otomo, T., Higaki, K., Nanba, E., Ozono, K. and Sakai, N. (2011) Lysosomal storage causes cellular dysfunction in mucolipidosis II skin fibroblasts. *J. Biol. Chem.*, **286**, 35283–35290.